Journal of Biomechanics 83 (2019) 49–56

Contents lists available at ScienceDirect

Journal of Biomechanics

journal homepage: www.elsevier.com/locate/jbiomech
www.JBiomech.com

Virtual structural analysis of tibial fracture healing from low-dose clinical CT scans

Peter Schwarzenberg [a,*], Michael M. Maher [b], James A. Harty [c], Hannah L. Dailey [a]

[a] Department of Mechanical Engineering and Mechanics, Lehigh University, Bethlehem, PA, USA
[b] Department of Radiology, Cork University Hospital, University College Cork, Wilton, Cork, Ireland
[c] Department of Orthopaedic Surgery, Cork University Hospital, University College Cork, Wilton, Cork, Ireland

ARTICLE INFO

Article history:
Accepted 12 November 2018

Keywords:
Tibial shaft fracture
Intramedullary nailing
Computed tomography
Subject-specific finite element modeling

ABSTRACT

Quantitative assessment of bone fracture healing remains a significant challenge in orthopaedic trauma research. Accordingly, we developed a new technique for assessing bone healing using virtual mechano-structural analysis of computed tomography (CT) scans. CT scans from 19 fractured human tibiae at 12 weeks after surgery were segmented and prepared for finite element analysis (FEA). Boundary conditions were applied to the models to simulate a torsion test that is commonly used to access the structural integrity of long bones in animal models of fracture healing. The output of each model was the virtual torsional rigidity (VTR) of the healing zone, normalized to the torsional rigidity of each patient's virtually reconstructed tibia. This provided a structural measure to track the percentage of healing each patient had undergone. Callus morphometric measurements were also collected from the CT scans. Results showed that at 12 weeks post-op, more than 75% of patients achieved a normalized VTR (torsional rigidity relative to uninjured bone) of 85% or above. The predicted intact torsional rigidities compared well with published cadaveric data. Across all patients, callus volume and density were weakly and non-significantly correlated with normalized VTR and time to clinical union. Conversely, normalized VTR was significantly correlated with time to union ($R^2 = 0.383$, $p = 0.005$). This suggests that fracture scoring methods based on the visual appearance of callus may not accurately predict mechanical integrity. The image-based structural analysis presented here may be a useful technique for assessment of bone healing in orthopaedic trauma research.

1. Introduction

In clinical studies of bone healing, progress is usually tracked using subjective assessments such as pain and mobility scores, clinical assessments of X-rays, and recorded complications such as nonunions, implant fatigue failures, and reoperations. These research designs are significantly limited by the variability of the data produced and lack of statistical power. For example, in one large device-related trial pertaining to angular-stable fixation of distal tibia fractures, patient- reported pain levels were highly variable and showed a strong trend toward decreasing pain over time without a detectable difference in pain between the groups based on fixator type (Höntzsch et al., 2014). When studies focus on relatively rare complications, such as nonunion or reoperation, very large multi-center trials with thousands of cases are needed to detect differences between groups, such as in the SPRINT study on reamed versus un-reamed tibial nailing (Bhandari et al., 2008).

A lack of consistency in the evaluation of fracture healing has been a widely recognized clinical problem in orthopaedic trauma (Bhandari et al., 2002) and the need for greater objectivity led to the development of the radiographic union scale for tibial fractures (RUST). The RUST X-ray scoring system evaluates visible callus at each of the four cortices to assess healing progress (Whelan et al., 2010). The RUST approach has demonstrable intra- and inter-observer reliability (Leow et al., 2016; Whelan et al., 2010), has been adapted for use in metaphyseal fractures (Litrenta et al., 2015), and has become a commonly used tool in the design of randomized controlled trials (Castillo et al., 2017). The advantage of RUST scoring is that it was designed to capture the development of external callus at the fracture site and has demonstrated utility as a tool to differentiate between united and nonunited fractures (RUST > 10 for union) in clinical studies (Bishop et al., 2012; O'Halloran et al., 2016; Van Houten et al., 2014). However, RUST

* Corresponding author at: Department of Mechanical Engineering & Mechanics, Packard Laboratory, Room 356, 19 Memorial Drive West, Bethlehem, PA 18015, USA.
E-mail address: Peter@lehigh.edu (P. Schwarzenberg).

https://doi.org/10.1016/j.jbiomech.2018.11.020
0021-9290/

scores are not objective and interpretation of the scoring criteria can be ambiguous, leading to known difficulties in inter-rater agreement (Leow et al., 2016). Some recent efforts to introduce objectivity in healing assessment have included image analysis techniques for measuring callus from 2D plain film X-rays (Porter et al., 2016), but the results from these methods are not a measure of structural mechanics at the fracture site.

In contrast, preclinical research has demonstrated the power of 3-D imaging to assess not just callus presence and connectivity, but also the material properties and complex geometry that together define the objective structural integrity of the callus region. Methods developed for ovine studies have been shown to successfully monitor the *in vivo* bone adaptive response within an individual animal *in silico* utilizing computed tomography (CT) scan data (Jaecques et al., 2004). The published history of CT-based analysis of fracture healing includes simplistic structural studies that idealized the fracture as basic geometric shapes to approximately calculate strength (Morgan et al., 2009). Additionally, methods have been developed to assign element-wise material properties for finite element (FE) models (Chen et al., 2010; Gao et al., 2013; Shefelbine et al., 2005). However, these studies have not been conducted in humans because post-mortem high-resolution micro-CT scanning is not translatable to clinical research designs. Accordingly, the purpose of this study was to develop a robust method for carrying out structural evaluation of fracture healing using low-dose CT scans of clinical fractures treated by routine surgical fracture fixation.

2. Methods

2.1. Clinical study information

A sequential cohort of N = 19 tibial fracture patients was prospectively recruited from Cork University Hospital, a Level I trauma centre located in Cork, Ireland. The primary inclusion criteria were diaphyseal or proximal/distal extra-articular tibial fractures (AO/OTA 41-A2/A3, 42-A, 42-B, 42-C, and 43A) in patients 18 years of age or older and deemed clinically suitable for reamed intramedullary nail fixation. The protocol for this study was reviewed and approved by the local Institutional Review Board and all patients provided written informed consent. Exclusion criteria included but were not limited to chronic disease, osteoporosis, pregnancy, polytrauma, deformity or previous metalwork. All tibial nails were statically interlocked with two proximal and two distal screws. For each case, the injury severity is characterized as closed or open. The OTA/AO classification is also given as a reference to the system of morphological characterization used by surgeons to describe fractures. Table 1 outlines summary data for each patient. All cases were reviewed at a minimum of one year follow-up.

2.2. Radiology protocols

Low-dose CT scans were performed 12 weeks after surgery. CT scans were performed on a GE (General Electric Healthcare; WI, USA) Discovery CT750 HD with X-ray tube voltage of 80 kV, current-time product of 10mAs, gantry rotation speed of 0.4 s, and a pitch of 0.52. A pure iterative reconstruction algorithm, Model-Based Iterative Reconstruction (MBIR), Veo (General Electric Healthcare) was used for image reconstruction with a resolution improvement, RP05, filter kernel (Li et al., 2016; Li et al, 2014). The resulting scan resolution had a slice thickness of 0.625 mm and a median pixel spacing of 0.373 mm (Fig. 1a). RUST scores were determined from conventional X-rays taken at 12 weeks, with the observer blinded to the CT analysis.

2.3. Scan processing and injured limb reconstruction

A segmentation workflow (Fig. 1) using the Mimics Innovation Suite (Materialise, Leuven, Belgium) was used to create 3D surface models by applying density-based threshold rules to the CT scan images, selecting cohesive regions of voxels that represent different tissues (Fig. 1b). For this study, threshold values of 400–1400 Hounsfield Units (HU) were chosen to segment the callus and values of 1400–2700 HU were chosen to segment cortical bone. The lower bound was chosen by first applying a 50/50 mixing rule of woven bone and cartilage as a baseline assumption (Ament and Hofer, 2000). This threshold was then increased until the non-callus surrounding soft tissue was no longer being captured for several representative scans. The resulting 400 HU threshold was then uniformly applied for all models. For the upper bound (2700 HU), the threshold was set to inclusively capture cortical bone without capturing any voxels from the high-density intramedullary nail. Lastly, the division between existing cortical bone and new callus (1400 HU) was chosen by varying the cutoff and visually inspecting models from several representative scans for any non-physical features at the fracture site, such as non-physical voids or outgrowths in the cortical bone.

A parameter sensitivity study was used to investigate the influence each chosen threshold had on the resulting geometric models. A ± 100 HU variation in the upper threshold value produced a percent volume change of less than 2% for cortical bone. Varying the middle threshold by ±100 HU resulted in a percent change in volume of less than 6% in the callus region and less than 4% in the existing cortical bone. While the variation of the middle threshold value may change the morphometric parameters, the final unified structural model remains the same. Lastly, a lower threshold variation of ±100 HU had a percent change in volume of less than 20% on the callus region. The lower threshold has the most potential to be problematic because the tissue density becomes comparable to that of the soft tissue envelope and can produce obvious non-physical segmented geometry features on the callus. Even though the sensitivity is high, the rationale for the set point is based on choosing a minimum cutoff that produces a clinically relevant structure.

In preparation for volumetric discretization, a series of surface cleanup operations were performed to optimize the outer envelope of each segmented region. Region growing and morphometric erosion and dilation tools were used to refine the segmented cortical bone and callus regions from each scan (Fig. 1c). These regions were unified into a single body and cut surfaces were created just distal to the proximal screws and just proximal to the distal screws in preparation for finite element (FE) boundary condition (BC) application. The choice of cut surface location is equivalent to the working length typically used in physical mechanical testing of preclinical defect models. The final unified surface was smoothed to minimize CT noise from the scanning process and improve meshability. Smoothing produced less than a 0.25% change in volume.

2.4. Finite element model creation

Meshing for FE structural mechanics was carried out using a dedicated toolkit in Mimics, 3-Matic. First, a triangular surface mesh was created on the unified surface body, then volumetric discretization was completed using tetrahedral-4 elements. The meshing control parameters were as follows: surface mesh maximum edge length was 0.4 mm and interior mesh maximum edge length was 0.875 mm. These settings were selected based on a mesh dependency analysis in which the criteria for acceptance was <1% change in fractured limb torsional rigidity. After meshing, element-wise mechanical properties were interpolated from voxel

Table 1
Patient data for all CT scans.

CT case number [–]	Gender [Male/Female]	Age [Years]	Injury [Closed/Open]	OTA/AO [–]
CT01	Female	51	Closed	42A2
CT02	Male	52	Closed	42A1
CT03	Male	32	Open	42B3
CT04	Male	32	Closed	42A3
CT05	Male	55	Closed	42A1
CT06	Male	58	Closed	42A3
CT07	Male	33	Closed	42A2
CT08	Female	39	Open	42B2
CT09	Male	65	Closed	42C2
CT10	Male	33	Closed	42A3
CT11	Male	20	Closed	42A3
CT12	Male	45	Open	42A2
CT13	Male	50	Closed	42A1
CT14	Male	24	Closed	42A1
CT15	Male	39	Closed	42A2
CT16	Male	29	Closed	42A3
CT17	Male	57	Closed	42B3
CT18	Male	53	Closed	42A1
CT19	Male	18	Closed	42A3

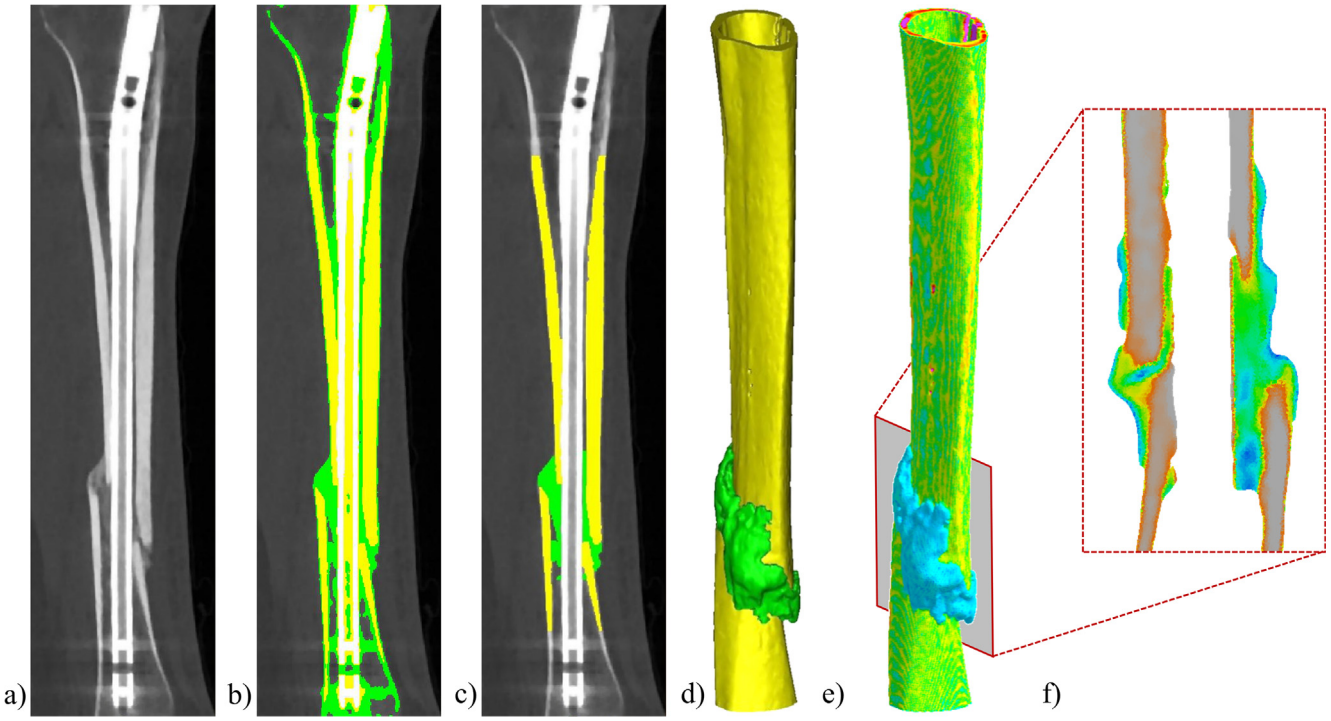

Fig. 1. (a) Sagittal slice view of CT DICOM stack without masks applied. (b) Sagittal view with bone (yellow 1400–2700 HU) and callus (green 400–1400 HU) thresholds applied. (c) Sagittal slice view with bone and callus thresholds after morphometric tools applied. (d) 3D surface model after morphometric tools applied. This model is discretized and meshed to create a finite element mesh. (e) Elastic modulus contour plot of finite element material assignment. (f) Section view of callus region. All elements corresponding to a HU value above 1400 were set to gray. (For interpretation of the references to colour in this figure legend, the reader is referred to the web version of this article.)

image intensities using a previously published elastic modulus scaling law based on local Hounsfield units of the original CT scan: $E = 0.00704 \times HU$ GPa (Snyder and Schneider, 1991). Six representative models of finite element meshes with applied elastic moduli can be seen in Fig. 2.

2.5. Reconstructed finite element models

Within the group of individuals recruited for this study, considerable variations were observed in stature, bone quality, and cortical bone thickness. These parameters all influence the expected torsional stiffness of the pre-injured bone and confound the comparison between individuals at the 12-week time point. To minimize the between-individuals differences that were unrelated to the injury pattern and healing response, each individual's cortical bone fragments were digitally reconstructed to form a virtual intact model. To reconstruct each fracture limb, image sets were segmented to identify only old cortical bone (Fig. 3a). The resulting surface models were then virtually realigned to match an anatomically intact tibia (Fig. 3b). The cortical bone fragments were united by applying wrapping and gap closing function to create a single enclosed surface and a volumetric mesh was created using the

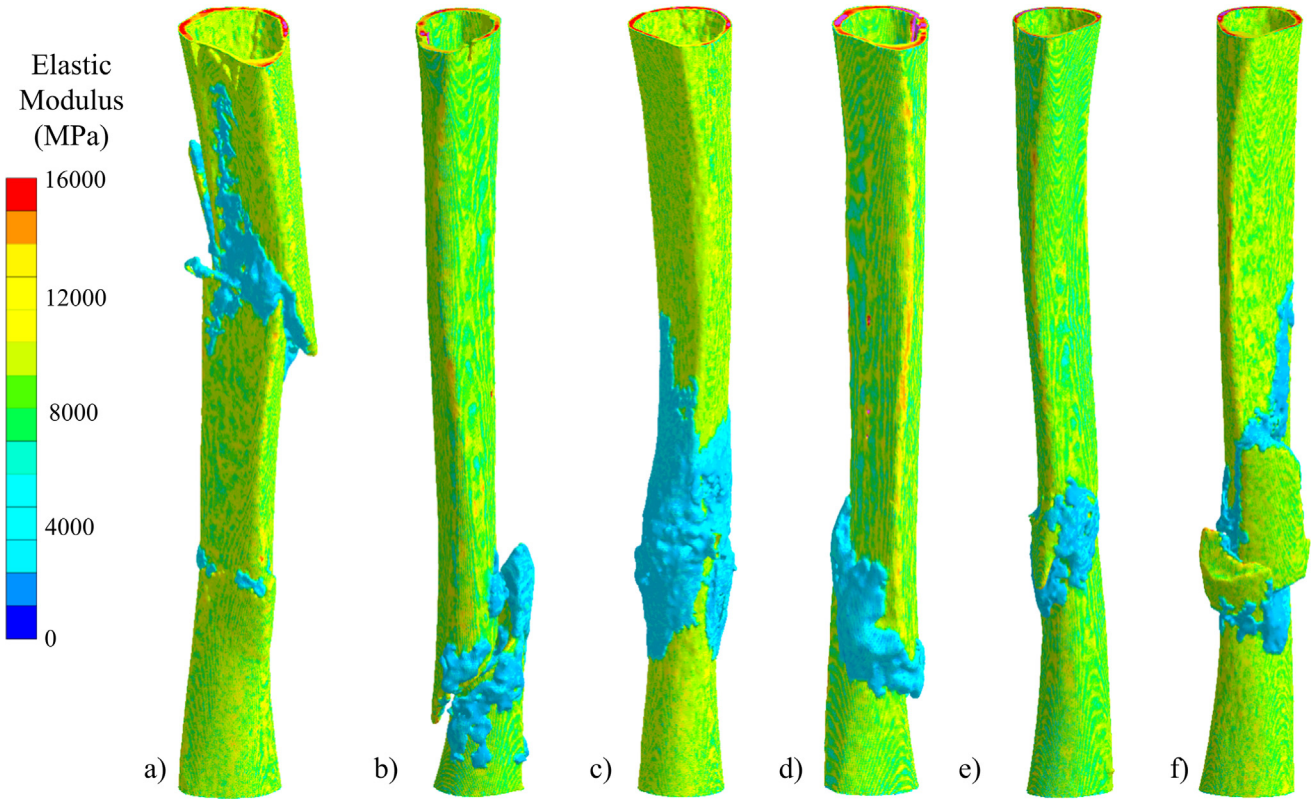

Fig. 2. Elastic modulus contour plots of finite element models with AO/OTA fracture classification. Moduli above scale are plotted in purple. (a) CT09: 42-C2 Complex Fracture Segmental. (b) CT13: 42-A2 Simple Fracture – Oblique Delayed Union Outlier Fracture (c) CT11: 42-A3 Simple Fracture – Transverse. (d) CT01: 42-A2 Simple Fracture – Oblique. (e) CT04: 42-B3 Wedge Fracture – Fragmented Wedge. (f) CT03: 42-C3 Complex Fracture – Irregular. (For interpretation of the references to colour in this figure legend, the reader is referred to the web version of this article.)

same parameters as in the fracture models (Fig. 3c). The realignment process eliminated the option of voxel-derived elementwise moduli, so the median HU value was used to assign a homogenous Young's modulus.

2.6. Virtual torsion testing

In preclinical models of fracture healing, torsional rigidity is a commonly used rotational stiffness parameter that results from a single post-mortem mechanical test. Torsional rigidity relative to intact paired controls is generally used as a summary index of healing progress because these tests are destructive, so only one measurement can be performed. Although some investigators have chosen to report bending stiffness as a summary structural measure, bending stiffness is highly affected by the rotational orientation of the tibia during testing, whereas torsional stiffness is not (Augat et al., 2008). For this investigation, we calculated virtual torsional rigidity (VTR) to mimic *in vitro* torsional tests. VTR is defined as the moment reaction from the applied loading (M) multiplied by the length of the test segment (L) divided by the resultant angle of twist (ϕ): $VTR = ML/\phi$ [N m^2/°].

All structural simulations were carried out in ANSYS 17.2 and FE meshes created in Mimics were imported into ANSYS with elementwise material properties for the fracture model and homogeneous properties for the virtually reconstructed intact models. Boundary conditions were applied as follows: rigid fixation on the distal end and 1 degree of rotation on the proximal end about the mechanical axis of the tibia. The static structural model was then solved and moment reactions at the distal face were reported to allow calculation of VTR. This virtual torsion test was repeated for both the injured limb models and the reconstructed intact models. A linearity study showed that VTR changed by less than 1% up to 10 degrees of applied angle of twist. VTR of each fractured model was then normalized to the reconstructed models to help remove individual anatomical variation between patients.

2.7. Statistical analysis

Descriptive statistics were generated using Microsoft Excel (2016) and MATLAB (R2016a, The MathWorks, Inc., Natick, Massachusetts). Unless otherwise indicated, values are reported as medians and interquartile ranges. Additional statistical analysis was conducted in SPSS 24.0 (IBM Corp., Armonk, NY). Correlations between various morphometric and structural parameters were assessed using Pearson's correlation coefficient. Multiple regressions were also performed between outcome parameters of fractured VTR and normalized VTR and independent parameters of median callus density, callus volume, and median bone density.

3. Results

3.1. Clinical outcomes

Median time to clinical union was 18.7 (15.7–26.1) weeks. One individual experienced a delayed union, as indicated clinically by progressive autodynamization and eventual union at 38 weeks. Another individual was followed up for an extended period (48 weeks) but did not experience any hardware failures. Median RUST score at 12 weeks was 11 (8–12).

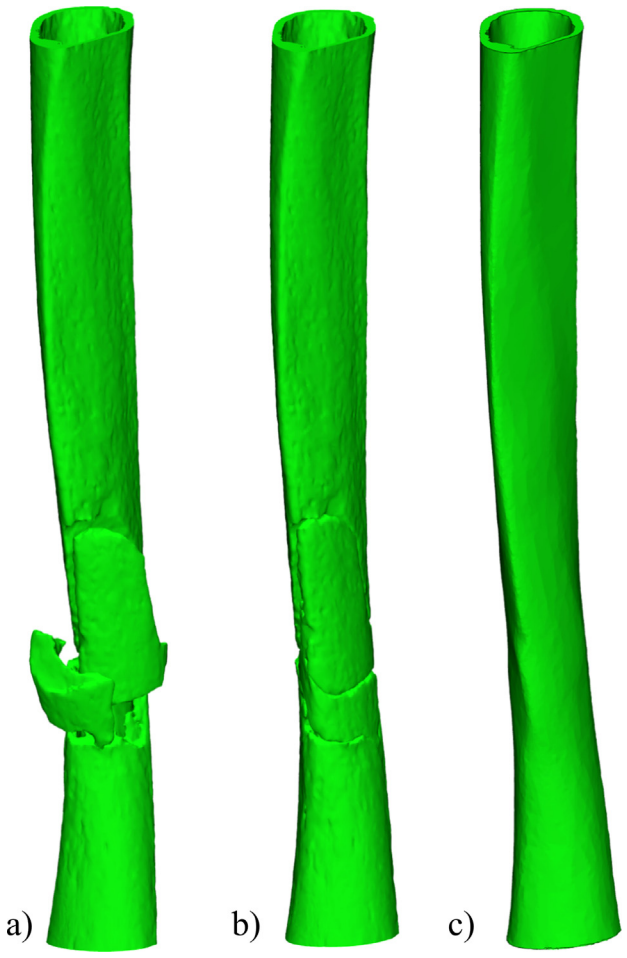

Fig. 3. (a) CT03 existing cortical bone before reconstruction. (b) CT03 existing cortical bone after reconstruction alignment. (c) CT03 wrapped reconstructed model.

3.2. Morphometric data

For each individual, the distributions of radiodensity in both the callus and cortical bone were all non-normally distributed by the Kolmogorov-Smirnov test (all $p > 0.05$), so the median Hounsfield Unit was reported for each model in each tissue zone. The median callus density across all models was 772 (722–799.5) HU (Fig. 4a). The median callus volume across the 19 fracture models was 9.13 (8.16–14.49) cm^3 (Fig. 4b). The median number of elements in each FE model was 5,679,666 (4,453,970–6,296,804) tetrahedral-4 elements. Table 2 outlines the results for each patient case.

3.3. Structural data: VTR

Virtual torsional rigidity (VTR) was calculated for each fracture model and had a median value of 2.09 (1.65–2.66) N $m^2/°$. The median VTR for the virtually reconstructed intact models was 2.09 (1.78–2.77) N $m^2/°$. The fractured models were normalized to their own reconstructed model to calculate a normalized VTR value representing how each patient's healing has progressed. The normalized VTR was found to be 0.99 (0.86–1.13) [–] (Fig. 4c).

3.4. Statistical correlations

Statistical correlation analysis was used to assess whether clinically relevant observable relationships may exist between any of the morphometric and structural healing measures. For this analysis, four measures were considered: callus volume, callus density, virtual torsional rigidity (VTR) of the fractured tibia, and VTR of the reconstructed intact bone models. First, we considered the relationship between callus density and VTR of the fractured bone (Fig. 5a). This correlation was weak and non-significant ($R^2 = 0.0001$, $p = 0.961$). Next, we considered the relationship between callus volume and VTR of the fracture bone (Fig. 5b). This correlation was also weak and non-significant ($R^2 = 0.02$, $p = 0.561$). Fractured VTR was strongly correlated with reconstructed VTR ($R^2 = 0.594$, $p < 0.001$, Fig. 5c). Multiple regressions were run to predict normalized VTR and time to clinical union from three simple CT measures: callus density, callus volume, and bone density. Both regressions were non-significant ($R^2 = 0.170$, $p = 0.226$; $R2 = 0.300$, $p = 0.137$ respectively).

4. Discussion

Traditional radiographic assessment of fracture healing has relied on human subjective interpretation of the quantity and quality of visible callus on X-rays, assuming that denser-looking callus indicates a stiffer healing zone. Qualitatively, this may be true, but the quantitative data presented in this work shows that observations about callus size or density do not necessarily independently predict the structural integrity of the partially healed bone. In this study, we found that morphometric measures (e.g. callus volume and density) have a weak and non-significant correlation with torsional rigidity, both individually and in multiple regression analy-

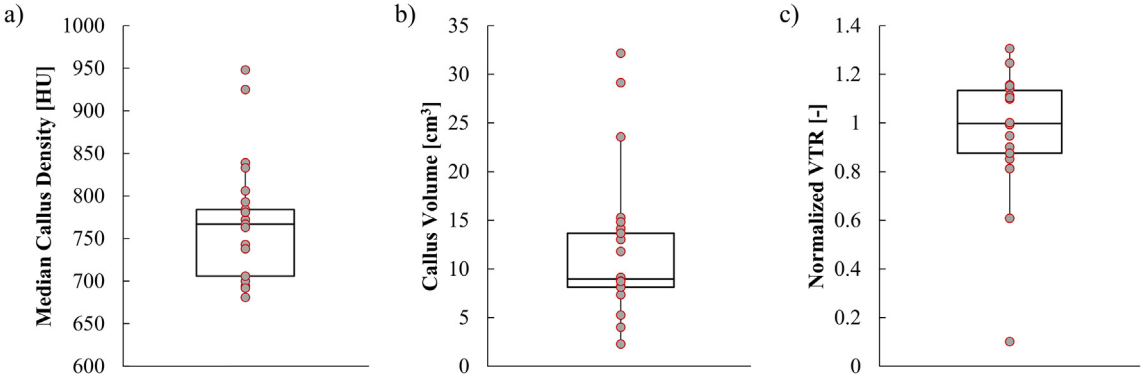

Fig. 4. (a) Distribution of median callus density of each model measured from gray values of original DICOM CT scans (772 (722–799.5) HU). (b) Distribution of the callus volume of each model measured from 3D surface body created (9.13 (8.16–14.49) cm^3). (c) Distribution of fractured limb VTR normalized to reconstructed VTR (0.99 (0.86–1.13)).

Table 2
Morphometric properties of the 19 patient models. Callus and bone density were calculated from Hounsfield Units of original CT scan data. Callus volume was calculated from the mask created in Mimics Innovation Suite. Number of elements is the number of tetrahedral-4 elements in each FE model. Length is the distance from distal to proximal surface.

CT case number	Median callus density		Callus volume	Median bone density		Number of elements	Working length	Fractured VTR	Reconstructed VTR	Normalized VTR
[–]	[HU]	[Q1–Q3]	[cm^3]	[HU]	[Q1–Q3]	[–]	[mm]	[N m^2/°]	[N m^2/°]	[–]
CT01	806	(622–1029)	7.35	2121	(1951–2270)	3.45E+06	202	1.48	1.28	1.16
CT02	694	(517–958)	14.2	2059	(1864–2210)	6.55E+06	269	3.66	3.21	1.14
CT03	743	(545–1032)	8.97	2034	(1844–2174)	5.81E+06	263	1.63	2.68	0.61
CT04	700	(552–949)	5.27	2062	(1877–2203)	5.68E+06	275	2.41	2.43	0.99
CT05	839	(584–1103)	15.3	1737	(1612–1918)	4.10E+06	189	1.94	1.48	1.31
CT06	738	(532–1070)	8.20	1926	(1753–2065)	4.42E+06	230	1.37	1.68	0.81
CT07	782	(580–1053)	9.13	1940	(1786–2081)	7.30E+06	291	4.06	3.70	1.10
CT08	772	(579–1006)	8.12	2053	(1842–2235)	1.17E+05	265	1.73	1.73	1.00
CT09	767	(560–1060)	32.2	1984	(1783–2121)	7.26E+06	261	2.82	3.31	0.85
CT10	925	(681–1165)	14.8	1916	(1722–2082)	4.39E+06	201	1.99	1.73	1.15
CT11	784	(591–1021)	23.6	2017	(1802–2196)	5.59E+06	251	2.61	2.09	1.25
CT12	706	(531–1008)	11.8	1954	(1784–2114)	6.12E+06	256	2.71	2.86	0.95
CT13	681	(531–920)	8.76	1961	(1773–2117)	5.19E+06	265	0.19	1.85	0.10
CT14	781	(584–1047)	2.29	1868	(1706–2027)	4.49E+06	231	2.09	1.88	1.11
CT15	793	(577–1050)	4.01	2069	(1904–2186)	5.77E+06	264	2.34	2.59	0.90
CT16	763	(580–1002)	8.72	2103	(1922–2219)	6.47E+06	268	2.60	3.20	0.81
CT17	692	(526–980)	13.0	1929	(1773–2074)	5.82E+06	259	1.68	1.91	0.88
CT18	948	(636–1234)	29.1	1732	(1573–1973)	5.15E+06	213	1.61	1.84	0.88
CT19	833	(604–1109)	13.7	1922	(1754–2070)	6.63E+06	276	2.83	2.56	1.10

sis. This is because both the geometry and material properties influence how the loading through the limb is distributed. Simply assessing the connectivity and volume of callus without including material mechanics does not accurately represent the complex structure of the healing zone. In some cases, these morphometric parameters can even misguide the determination of the healing progress, such as when a large volume of low-density callus is less stiff than a small volume of denser callus. The virtual mechanical test method we have developed combines material and shape to create a simple and intuitive measure of the structural progress toward full recovery.

Dealing with individual anatomic variations is a notable challenge in biomechanical studies. Previously published values for the torsional rigidity of intact cadaver tibiae indicate an expected mean value 2.42 ± 0.80 N m^2/° (Heiner, 2008), indicating that model results were within the expected physiological range. In this case series, the coefficient of variation for VTR of the reconstructed intact limbs was 29.3%, illustrating the significant anatomical differences observed between patients within this group. These variations are important to understand because they may confound interpretation of healing progress in the injured limb. This concern is supported by the fact that we observed a strong and statistically significant correlation between VTR of the fractured model and the reconstructed models, with a Pearson's correlation coefficient (R^2) of 0.594 ($p < 0.001$). To minimize the effect of these variations, VTR of each patient's fracture was normalized to their own reconstructed model. This normalization allowed a comparison of all 19 subjects to their own pre-fractured bone and insight into their individual healing process. The coefficient of variation of the normalized VTR for all 19 cases in this series was 27.6%. Although the normalized VTR has similar variability to the non-normalized VTR, the process of referencing each model to its own intact bone minimizes variations arising from anatomy to focus on the fracture pattern and healing response.

The central premise of this study was that a virtual mechanical analysis technique may be useful for characterizing the typical fracture healing response of a cohort of similarly managed cases. Fig. 4c shows that in our cohort, more than 75% of patients (first quartile and above) achieved a torsional rigidity equivalent to at least 85% of their intact limb at 12 weeks. In this cohort, there was only one fracture model that was an outlier using Tukey's inner fence criteria, with a normalized VTR of 10%. This patient experienced a delayed union, characterized by progressive autodynamization (screw breakage) and final union at 38 weeks.

An advantage of the VTR method is that the minimization of individual anatomical variations makes the resulting outcome parameter statistically powerful and could allow for smaller recruitment targets for clinical studies. For example, to detect a difference of 20% between two hypothetical treatment groups at 80% power and a significance level of 0.05, outcomes assessments based on callus volume would require sample sizes of 151 patients per group compared to only 30 patients to detect the same differences in normalized VTR. By these measures, VTR allows new and powerful insight into the biomechanical tissue-adaptation response to osteosynthesis and introduces an intuitive new outcome measure that could be used to detect differences between patient groups with much smaller recruitment targets than are currently the norm. Studies that investigate topics such as patient risk factors, surgical implant selection, surgical technique, or post-operative rehabilitation could greatly benefit from inclusion of this method as part of the study design.

This investigation has a few noteworthy limitations. First, the torsional rigidity of human fractured tibiae cannot be measured by any direct physical means to validate the VTR of the 12 weeks scans. However, the calculated torsional rigidities of the recon-

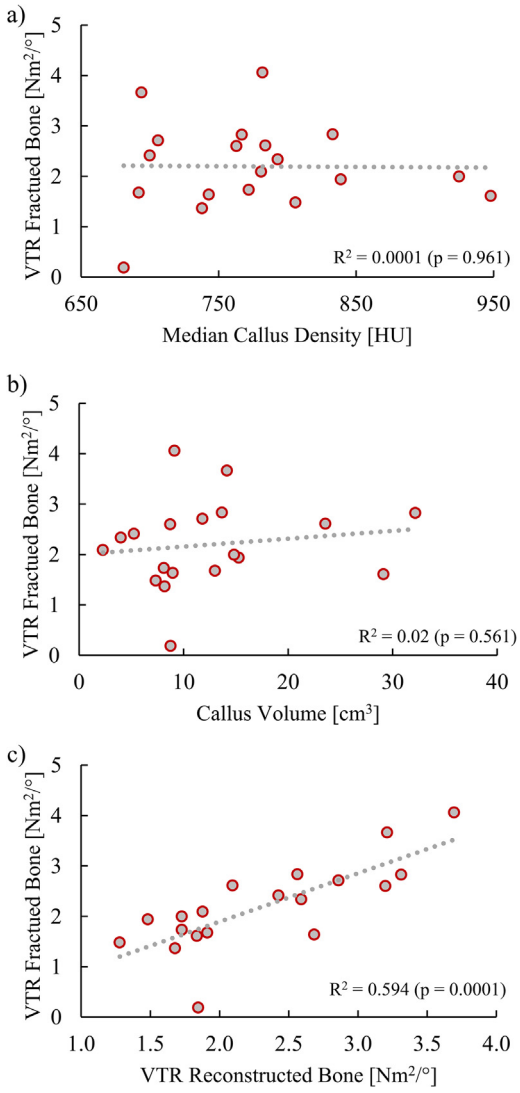

Fig. 5. (a) Scatter plot of callus volume vs VTR of reconstructed bone. (b) Scatter plot of callus density vs. VTR of reconstructed bone. (c) Scatter plot of VTR of fractured limb vs. VTR of reconstructed bone.

structed intact limbs are within the range of previously reported values for intact cadaver tibiae (Heiner, 2008). Another limiting factor in these patient-specific models with element-wise density-based mechanical properties is the limited availability of validated Young's modulus scaling laws for the tissues that are relevant for fracture healing. While there are many distinct models to predict elastic moduli of cortical and trabecular bone regions based on density measurements from image analyses, there is little agreement between these models and understandably little data on numerical models for new bone growth in the callus region (Tuncer et al., 2014). For our study, the same scaling power law scaling was applied for all patients using the equation $E = HU \times 0.00704$ GPa. (reported as $E = 70.4 \times 10^5 \times HU$) (Snyder and Schneider, 1991). This scaling law is not necessarily the only appropriate or best option, particularly as it does not address callus viscoelasticity, but it was applied consistently across all patients as part of a controlled model-generation workflow.

Researchers intending to use these techniques should employ judicious caution when interpreting the results, recognizing that differences in scanner settings, image segmentation protocols, and material property assignments may all influence the results obtained. However, strict protocol adherence ensures that the models will be useful as a comparative tool for assessing between- and within-group variations in clinical orthopaedic trauma research.

5. Conclusions

Image-based structural mechanics modeling from low-dose CT is a robust, repeatable, objective, quantitative, and powerful approach to assessing fracture healing in clinical orthopaedic trauma research. Using the methods described above, we were able to quantitatively access the structural progress of fracture healing compared to each patient's own intact bone. The results provide insights into fracture healing that are not possible with the suite of qualitative and semi-quantitative observational measures typically used in clinical studies. These semi-quantitative measures, such as volume, can even lead to incorrect conclusions about a patient's healing. The virtual torsional rigidity technique also shows much lower variability than traditional morphometric data and may enable hypothesis testing in orthopaedic trauma research with much smaller recruitment targets.

Acknowledgements

Institutional support for this work was provided by Lehigh University and Cork University Hospital. The authors gratefully acknowledge contributions from Karl James MB, FFR (RCSI), Richard Kavanagh MB, FFR (RCSI), and Owen J. O'Connor MB, FFR (RCSI).

Conflict of interest statement

HLD and JAH have stock or stock options in OrthoXel, DAC. No OrthoXel devices were used in this study. For the remaining authors, no conflicts were declared.

Appendix A. Supplementary material

Supplementary data to this article can be found online at https://doi.org/10.1016/j.jbiomech.2018.11.020.

References

Ament, C., Hofer, E., 2000. A fuzzy logic model of fracture healing. J. Biomech. 33, 961–968. https://doi.org/10.1016/S0021-9290(00)00049-X.

Augat, P., Penzkofer, R., Nolte, A., Maier, M., Panzer, S., Oldenburg, G.V., Pueschl, K., Simon, U., Bühren, V., 2008. Interfragmentary movement in diaphyseal tibia fractures fixed with locked intramedullary nails. J. Orthop. Trauma 22, 30–36. https://doi.org/10.1097/BOT.0b013e31816073cb.

Bhandari, M., Guyatt, G., Walter, S.D., Tornetta, P., Schemitsch, E.H., Swiontkowski, M., Sanders, D., 2008. Randomized trial of reamed and unreamed intramedullary nailing of tibial shaft fractures. J. Bone Jt. Surg. – Ser. A 90, 2567–2578. https://doi.org/10.2106/JBJS.G.01694.

Bhandari, M., Guyatt, G.H., Swiontkowski, M.F., Paul Tornetta, I., Sprague, S., Schemitsch, E.H., 2002. A lack of consensus in the assessment of fracture healing among orthopaedic surgeons. J. Orthop. Trauma 16, 562–566. https://doi.org/10.1097/01.BOT.0000031144.58425.CB.

Bishop, J.A., Palanca, A.A., Bellino, M.J., Lowenberg, D.W., 2012. Assessment of compromised fracture healing. J. Am. Acad. Orthop. Surg. 20, 273–282. https://doi.org/10.5435/JAAOS-20-05-273.

Castillo, R.C., Raja, S.N., Frey, K.P., Vallier, H.A., Tornetta, P., Jaeblon, T., Goff, B.J., Gottschalk, A., Scharfstein, D.O., O'Toole, R.V., Allen, L.E., Carlini, A.R., De Lissovoy, G., MacKenzie, E.J., Taylor, T.J., Weng, Y., 2017. Improving pain management and long-term outcomes following high-energy orthopaedic trauma (pain study). J. Orthop. Trauma 31, S71–S77. https://doi.org/10.1097/BOT.0000000000000793.

Chen, G., Schmutz, B., Epari, D., Rathnayaka, K., Ibrahim, S., Schuetz, M.A., Pearcy, M. J., 2010. A new approach for assigning bone material properties from CT images into finite element models. J. Biomech. 43, 1011–1015. https://doi.org/10.1016/j.jbiomech.2009.10.040.

Gao, J., Gong, H., Huang, X., Fang, J., Zhu, D., Fan, Y., 2013. Relationship between microstructure, material distribution, and mechanical properties of sheep tibia during fracture healing process. Int. J. Med. Sci. 10, 1560–1569. https://doi.org/10.7150/ijms.6611.

Heiner, A.D., 2008. Structural properties of fourth-generation composite femurs and tibias. J. Biomech. 41, 3282–3284. https://doi.org/10.1016/j.jbiomech.2008.08.013.

Höntzsch, D., Schaser, K.D., Hofmann, G.O., Pohlemann, T., Hem, E.S., Rothenbach, E., Krettek, C., Attal, R., 2014. Evaluation of the effectiveness of the angular stable locking system in patients with distal tibial fractures treated with intramedullary nailing: a multicenter randomized controlled trial. J. Bone Jt. Surg. – Am. Vol. https://doi.org/10.2106/JBJS.M.01355.

Jaecques, S.V.N., Van Oosterwyck, H., Muraru, L., Van Cleynenbreugel, T., De Smet, E., Wevers, M., Naert, I., Vander Sloten, J., 2004. Individualised, micro CT-based finite element modelling as a tool for biomechanical analysis related to tissue engineering of bone. Biomaterials 25, 1683–1696. https://doi.org/10.1016/S0142-9612(03)00516-7.

Leow, J.M., Clement, N.D., Tawonsawatruk, T., Simpson, C.J., Simpson, A.H.R.W., 2016. The radiographic union scale in tibial (RUST) fractures: reliability of the outcome measure at an independent centre. Bone Jt. Res. 5, 116–121. https://doi.org/10.1302/2046-3758.54.2000628.

Li, G., Liu, X., Dodge, C.T., Jensen, C.T., Rong, X.J., 2016. A noise power spectrum study of a new model-based iterative reconstruction system : Veo 3. 0. J. Appl. Clnical Med. Phys. 17, 428–439.

Li, K., Tang, J., Chen, G.-H., 2014. Statistical model based iterative reconstruction (MBIR) in clinical CT systems: Experimental assessment of noise performance. Med. Phys. 41, 041906. https://doi.org/10.1118/1.4867863.

Litrenta, J., Tornetta, P., Mehta, S., Jones, C., O'Toole, R.V., Bhandari, M., Kottmeier, S., Ostrum, R., Egol, K., Ricci, W., Schemitsch, E., Horwitz, D., 2015. Determination of radiographic healing: an assessment of consistency using RUST and modified RUST in metadiaphyseal fractures. J. Orthop. Trauma 29, 516–520. https://doi.org/10.1097/BOT.0000000000000390.

Morgan, E.F., Mason, Z.D., Chien, K.B., Pfeiffer, A.J., Barnes, G.L., Einhorn, T.A., Gerstenfeld, L.C., 2009. Micro-computed tomography assessment of fracture healing: relationships among callus structure, composition, and mechanical function. Bone 44, 335–344. https://doi.org/10.1016/j.bone.2008.10.039.

O'Halloran, K., Coale, M., Costales, T., Zerhusen, T., Castillo, R.C., Nascone, J.W., O'Toole, R.V., 2016. Will my tibial fracture heal? Predicting nonunion at the time of definitive fixation based on commonly available variables. Clin. Orthop. Relat. Res. 474, 1385–1395. https://doi.org/10.1007/s11999-016-4821-4.

Porter, S.M., Dailey, H.L., Hollar, K.A., Klein, K., Harty, J.A., Lujan, T.J., 2016. Automated measurement of fracture callus in radiographs using portable software. J. Orthop. Res. https://doi.org/10.1002/jor.23146.

Shefelbine, S.J., Simon, U., Claes, L., Gold, A., Gabet, Y., Bab, I., Müller, R., Augat, P., 2005. Prediction of fracture callus mechanical properties using micro-CT images and voxel-based finite element analysis. Bone 36, 480–488. https://doi.org/10.1016/j.bone.2004.11.007.

Snyder, S.M., Schneider, E., 1991. Estimation of mechanical properties of cortical bone by computed tomography. J. Orthop. Res. 9, 422–431. https://doi.org/10.1002/jor.1100090315.

Tuncer, M., Hansen, U.N., Amis, A.A., 2014. Prediction of structural failure of tibial bone models under physiological loads: effect of CT density-modulus relationships. Med. Eng. Phys. 36, 991–997. https://doi.org/10.1016/j.medengphy.2014.04.006.

Van Houten, A.H., Heesterbeek, P.J.C., Van Heerwaarden, R.J., Van Tienen, T.G., Wymenga, A.B., 2014. Medial open wedge high tibial osteotomy: Can delayed or nonunion be predicted? Clin. Orthop. Relat. Res. 472, 1217–1223. https://doi.org/10.1007/s11999-013-3383-y.

Whelan, D.B., Bhandari, M., Stephen, D., Kreder, H., Mckee, M.D., Zdero, R., Schemitsch, E.H., 2010. Development of the radiographic union score for tibial fractures for the assessment of tibial fracture healing after intramedullary fixation. J. Trauma – Inj. Infect. Crit. Care 68, 629–632. https://doi.org/10.1097/TA.0b013e3181a7c16d.